Journal of Sound and Vibration (1999) **223**(2), 197–212
Article No. jsvi.1998.2138, available online at http://www.idealibrary.com on IDEAL®

ACOUSTIC ATTENUATION PERFORMANCE OF CIRCULAR EXPANSION CHAMBERS WITH EXTENDED INLET/OUTLET

A. SELAMET AND Z. L. JI
Department of Mechanical Engineering and The Center for Automotive Research, The Ohio State University, Columbus, OH 43210-1107, *U.S.A.*

(*Received* 16 *April* 1998, *and in final form* 1 *October* 1998)

The acoustic attenuation performance of circular expansion chambers with extended inlet/outlet is investigated. Three approaches are employed to determine the transmission loss: (1) a two-dimensional, axisymmetric analytical solution for the concentric configuration; (2) a three-dimensional computational solution based on the substructure boundary element–transfer impedance matrix technique; and (3) experiments on an extended impedance tube set-up with expansion chambers fabricated with fixed inlet, outlet, and chamber diameters, and varying lengths for the extended ducts and the chamber, and varying offset locations of the inlet and outlet. The transmission loss results from all three approaches are shown to agree well for the concentric configurations. The computational approach is also applied to determine the acoustic attenuation performance of asymmetric expansion chambers with extended inlet/outlet, which also compares well with the experiments. The effect of geometry (lengths of the extended ducts and expansion chamber, and the offset angles of the asymmetric configuration) on the multidimensional wave propagation and acoustic attenuation performance is discussed in detail.

1. INTRODUCTION

Expansion chambers with extended inlet/outlet exhibit a desirable acoustic attenuation performance as a combination of usually broad band domes of a simple expansion chamber and the resonant peaks of a quarter-wave resonator. Based on the plane wave assumption, the four-pole parameters of this configuration are available [1], which may be used to predict the transmission loss. The one-dimensional theory, however, excludes the effect of higher order modes. Thus, while yielding reasonable predictions at lower frequencies, this simplistic approach is expected to deviate from experimental results at higher frequencies. The effect of higher order modes on the acoustic attenuation of some related silencers has received considerable attention, including concentric [2, 3] and asymmetric expansion chambers [4–10], flow-reversing chambers [11, 12], and Helmholtz resonators [13]. For expansion chambers with extended inlet/outlet, Åbom [14] developed, utilizing the mode-matching technique, a general

0022–460X/99/220212 + 16 $30.00/0

three-dimensional analytical approach to evaluate the four-pole parameters which incorporated higher order modes and yielding endplates. The transmission loss for one specific configuration is shown to agree well with the experiments. The work, however, has chosen not to elaborate on the effect of geometry with respect to the acoustic attenuation of these configurations.

The analytical solution is not applicable to the expansion chambers with offset extended inlet/outlet ducts since the eigenfunctions of these configurations cannot be determined. Numerical techniques, however, such as the finite element method (FEM) and the boundary element method (BEM) can be used to predict the acoustic attenuation performance of the same configurations. Sahasrabudhe *et al.* [15] applied the substructure finite element technique to predict transmission loss of expansion chambers with coaxial, as well as offset extended inlet/outlet. The conventional single-domain BEM is not applicable directly to the expansion chambers with extended ducts of thin wall due to the presence of singular boundary, requiring the use of multi-domain BEM [16]. Ji *et al.* [17] developed a substructure boundary element–transfer impedance matrix technique which can be used to determine the acoustic attenuation of expansion chambers with extended duct(s).

The objective of the present study is (1) to present a two-dimensional axisymmetric analytical approach to determine the transmission loss of the circular concentric expansion chambers with extended inlet/outlet; (2) to investigate analytically, computationally and experimentally the effect of lengths of extended ducts and the chambers on the acoustic attenuation performance; and (3) to examine computationally and experimentally the effect of inlet/outlet locations on the wave propagation and attenuation. While the main emphasis and contribution of the work is on the multidimensional wave propagation and attenuation, the limiting case of the planar wave behavior is also simply superimposed to illustrate its application bounds as applied to the present configurations. The effect of viscosity and yielding walls are neglected in both analytical and computational studies, while mean flow is excluded from all approaches.

Following the Introduction, section 2 develops a two-dimensional axisymmetric analytical approach, and section 3 briefly describes the boundary element method. Section 4 compares the transmission loss results from the analytical, computational and experimental approaches, as well as the one-dimensional theory, and discusses the effect of geometry on the acoustic attenuation performance of expansion chambers with extended inlet/outlet. Section 5 concludes the study with some final remarks.

2. ANALYTICAL APPROACH

For the two-dimensional sound propagation in a circular, concentric annular rigid duct with inner radius a_1 and outer radius a, the solution to the Helmholtz equation [1]

$$\nabla^2 P + k^2 P = 0 \tag{1}$$

can be written as [14, 18, 19]

$$P(r, z) = \sum_{n=0}^{\infty} [A_n^+ \, \mathrm{e}^{-\mathrm{j}k_{nz}z} + A_n^- \, \mathrm{e}^{\mathrm{j}k_{nz}z}] \Psi_n(r), \tag{2}$$

where P is the acoustic pressure; k is the wavenumber; (r, z) are the cylindrical co-ordinates; $\mathrm{j} = \sqrt{-1}$ is the imaginary unit; A_n^+ and A_n^- are the modal amplitudes corresponding to waves travelling in the positive and negative z directions;

$$\Psi_n(r) = J_0(\beta_n r/a) - [J_1(\beta_n)/Y_1(\beta_n)] Y_0(\beta_n r/a) \tag{3}$$

is the eigenfuction, β_n is the root satisfying the radial boundary condition of

$$J_1(\beta_n a_1/a) - [J_1(\beta_n)/Y_1(\beta_n)] Y_1(\beta_n a_1/a) = 0, \tag{4}$$

and n denotes the radial mode number;

$$k_n = [k^2 - (\beta_n/a)^2]^{1/2} \tag{5}$$

is the axial wavenumber of the mode $(0, n)$. For a rigid duct, a propagating wave has $k > \beta_n/a$ so that k_n is real and $\mathrm{e}^{-\mathrm{j}k_{nz}z}$ does not decay in z; an evanescent wave has $k < \beta_n/a$ so that k_n is negative imaginary and $\mathrm{e}^{-\mathrm{j}k_{nz}z}$ decays exponentially in z. Note that for $a_1 = 0$ equation (4) reduces to $J_1(\alpha_n) = 0$, the root here being designated by α_n to distinguish from the root β_n. The eigenfunction of equation (3) now becomes $\Psi_n(r) = J_0(\alpha_n r/a)$ and the axial wavenumber $k_n = [k^2 - (\alpha_n/a)^2]^{1/2}$, which are identical to those of a simple circular duct, as expected.

From the linearized momentum equation, $\mathrm{j}\rho\omega U = -\partial P/\partial z$, the axial particle velocity can be obtained as

$$U(r, z) = \frac{1}{\rho\omega} \sum_{n=0}^{\infty} k_n (A_n^+ \, \mathrm{e}^{-\mathrm{j}k_{nz}z} - A_n^- \, \mathrm{e}^{\mathrm{j}k_{nz}z}) \Psi_n(r), \tag{6}$$

where ρ is the medium density, and ω is the angular frequency. For a circular concentric expansion chamber with extended inlet and outlet ducts, as shown in Figure 1, equations (2) and (6) will be used for sound pressures and particle velocities in regions A, B, C, D and E.

At the left wall of the chamber, the rigid endplate boundary condition

$$U_B|_{z_1 = -l_1} = 0 \quad (\text{on } S_B) \tag{7}$$

gives, by using the orthogonality of the eigenfunction,

$$B_n^+ = B_n^- \, \mathrm{e}^{-2\mathrm{j}k_{B,n}l_1}. \tag{8}$$

At the expansion, the continuity conditions reveal, for the pressure and velocity,

$$P_A|_{z_1=0} = P_C|_{z_1=0}, \quad U_A|_{z_1=0} = U_C|_{z_1=0} \quad (\text{on } S_A), \tag{9, 10}$$

$$P_B|_{z_1=0} = P_C|_{z_1=0}, \quad U_B|_{z_1=0} = U_C|_{z_1=0} \quad (\text{on } S_B). \tag{11, 12}$$

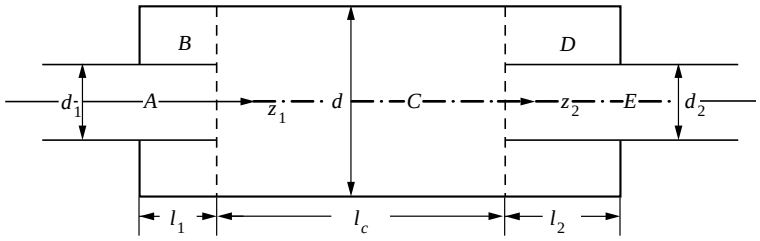

Figure 1. Circular expansion chamber with extended inlet and outlet ducts.

For the pressure continuity conditions, multiply both sides of equation (9) by $\Psi_{A,s}\,\mathrm{d}S$ and integrate over S_A to get, for $s = 0, 1, \ldots, \infty$,

$$(A_s^+ + A_s^-)\langle \Psi_{A,s}\Psi_{A,s}\rangle_A = \sum_{n=0}^{\infty}(C_n^+ + C_n^-)\langle \Psi_{C,n}\Psi_{A,s}\rangle_A; \tag{13}$$

multiply both sides of equation (11) by $\Psi_{B,s}\,\mathrm{d}S$ and integrate over S_B to get, for $s = 0, 1, \ldots, \infty$,

$$B_s^-(\mathrm{e}^{-2\mathrm{j}k_{B,s}l_1} + 1)\langle \Psi_{B,s}\Psi_{B,s}\rangle_B = \sum_{n=0}^{\infty}(C_n^+ + C_n^-)\langle \Psi_{C,n}\Psi_{B,s}\rangle_B; \tag{14}$$

where $\langle\ \rangle_s$ denotes the integration of an expression over S. For the two velocity continuity conditions, multiply both equations (10) and (12) by $\Psi_{C,s}\,\mathrm{d}S$ and integrate equation (10) over S_A and equation (12) over S_B, and then add these two integral equations to yield, for $s = 0, 1, \ldots, \infty$,

$$\sum_{n=0}^{\infty} k_{A,n}(A_n^+ - A_n^-)\langle \Psi_{A,n}\Psi_{C,s}\rangle_A + \sum_{n=0}^{\infty} k_{B,n}B_n^-(\mathrm{e}^{-2\mathrm{j}k_{B,n}l_1} - 1)\langle \Psi_{B,n}\Psi_{C,s}\rangle_B$$
$$= k_{C,s}(C_s^+ - C_s^-)\langle \Psi_{C,s}\Psi_{C,s}\rangle_C. \tag{15}$$

The integrals designated by $\langle\ \rangle$ in equations (13)–(15) are deferred to Appendix A.

At the right wall of the chamber, the rigid endplate boundary condition

$$U_D|_{z_2=l_2} = 0 \quad (\text{on } S_D) \tag{16}$$

gives, by using the orthogonality of the eigenfunction,

$$D_n^- = D_n^+\,\mathrm{e}^{-\mathrm{j}k_{D,n}l_2}. \tag{17}$$

At the contraction, the continuity conditions require, for the pressure and the velocity,

$$P_C|_{z_1=l_c} = P_E|_{z_2=0}, \quad U_C|_{z_1=l_c} = U_E|_{z_2=0} \quad (\text{on } S_E), \tag{18, 19}$$

$$P_C|_{z_1=l_c} = P_D|_{z_2=0}, \quad U_C|_{z_1=l_c} = U_D|_{z_2=0} \quad (\text{on } S_D). \tag{20, 21}$$

Using the same procedure as for the expansion, equation (18) gives, for $s = 0, 1, \ldots, \infty$,

$$\sum_{n=0}^{\infty}(C_n^+ \, \mathrm{e}^{-\mathrm{j}k_{C,n}l_c} + C_n^- \, \mathrm{e}^{\mathrm{j}k_{C,n}l_c})\langle \Psi_{C,n}\Psi_{E,s}\rangle_E = (E_s^+ + E_s^-)\langle \Psi_{E,s}\Psi_{E,s}\rangle_E; \tag{22}$$

equation (20) gives, for $s = 0, 1, \ldots, \infty$,

$$\sum_{n=0}^{\infty}(C_n^+ \, \mathrm{e}^{-\mathrm{j}k_{C,n}l_c} + C_n^- \, \mathrm{e}^{\mathrm{j}k_{C,n}l_c})\langle \Psi_{C,n}\Psi_{D,s}\rangle_D = D_s^+(1 + \mathrm{e}^{-2\mathrm{j}k_{D,s}l_2})\langle \Psi_{D,s}\Psi_{D,s}\rangle_D; \tag{23}$$

and equations (19) and (21) give, for $s = 0, 1, \ldots, \infty$,

$$k_{C,s}(C_s^+ \, \mathrm{e}^{-\mathrm{j}k_{C,n}l_c} - C_s^- \, \mathrm{e}^{\mathrm{j}k_{C,n}l_c})\langle \Psi_{C,s}\Psi_{C,s}\rangle_C = \sum_{n=0}^{\infty} k_{E,n}(E_n^+ - E_n^-)\langle \Psi_{E,n}\Psi_{C,s}\rangle_E + \sum_{n=0}^{\infty} k_{D,n}D_n^+(1 - \mathrm{e}^{-2\mathrm{j}k_{D,n}l_2})\langle \Psi_{D,n}\Psi_{C,s}\rangle_D. \tag{24}$$

The integrals designated by $\langle\ \rangle$ in equations (22)–(24) are also deferred to Appendix A. In comparison with Åbom, the present approach adds the two integral equations for the velocity continuity conditions (equations (10), (12) and (19), (21)) to get one analytical expression, at the expansion and contraction, respectively, thereby reducing the number of equations.

To determine the transmission loss of the expansion chamber with extended inlet and outlet ducts: (1) the dimensions of the inlet duct are assumed such that the incoming wave A^+ is planar, and its magnitude A_0^+ is chosen to be unity for convenience; and (2) an anechoic termination is imposed at the exit of the chamber by setting the reflected wave E_n^- to zero. Thus equations (13)–(15) and (22)–(24) can give a large (theoretically infinite) number of relations $6(s+1)$ for a large number of unknowns $6(n+1)$. The unknowns are the pressure magnitudes for incident and reflected waves in the regions A, B, C, D and E (A_n^-, B_n^-, C_n^+, C_n^-, D_n^+ and E_n^+). Since higher modes have a diminishing effect on the solution, s and n can be truncated to q resulting in $6(q+1)$ equations with $6(q+1)$ unknowns. The value of q needed for a converged solution depends on the magnitude of the area transition, the length of the chamber, and the frequency range of interest. For the geometries and frequencies investigated here, $q = 5$ were found to be sufficient. Once equations (13)–(15) and (22)–(24) are solved, the transmission loss is determined in the center of the outlet duct by

$$TL = -20\log_{10}\left|(a_2/a_1)\sum_{n=0}^{q} E_n^+ \, \mathrm{e}^{-\mathrm{j}k_{E,n}l_e}\right|. \tag{25}$$

Note that the non-propagating modes leaving the expansion chamber in the outlet duct will decay rapidly over the short distance l_e due to the smaller duct diameter. This distance is chosen so that the higher modes will have a negligible effect on the transmission loss calculations.

Setting $q = 0$ in equations (13)–(15) and (22)–(24) readily gives the classical transmission loss of a one-dimensional expansion chamber with extended inlet/outlet as

$$TL = 20 \log_{10} \frac{1}{4m} |[(m+1) + \mathrm{j}(m-1) \tan kl_1][(m+1) + \mathrm{j}(m-1) \tan kl_2] \, \mathrm{e}^{\mathrm{j}kl_c} - (m-1)^2 [1 - \mathrm{j} \tan kl_1][1 - \mathrm{j} \tan kl_2] \, \mathrm{e}^{-\mathrm{j}kl_c}|, \tag{26}$$

where $a_1 = a_2$ is used and $m = (a/a_1)^2$ is the ratio of cross-sectional areas.

3. BOUNDARY ELEMENT APPROACH

The boundary integral expression of Helmholtz equation (1) can be represented as [16]

$$C(X)P(X) = \int_\Gamma \left[G(X, Y) \frac{\partial P}{\partial n}(Y) - P(Y) \frac{\partial G}{\partial n}(X, Y) \right] \mathrm{d}\Gamma(Y), \tag{27}$$

here Γ is the boundary surface of the acoustic domain, n is the unit normal vector on Γ directed away from the domain, the function $G(X, Y) = \exp(-\mathrm{j}kR)/4\pi R$ is Green's function of free space, where R is the distance between any two points X and Y in the domain or on the surface, and $C(X)$ is a coefficient which depends on the position of point X.

A numerical solution of the boundary integral equation (27) can be achieved by discretizing the boundary surface of the domain into a number of elements. By using discretization and numerical integration, the following algebraic system of equations is obtained [16, 17]:

$$[\mathbf{H}]\{\mathbf{P}\} = [\mathbf{G}]\{\mathbf{U}_n\}, \tag{28}$$

where [**H**] and [**G**] are the coefficient matrices, and {**P**} and {$\mathbf{U}_n$} are the vectors whose elements are the acoustic pressure P and outward normal particle velocity U_n on the boundary nodes, respectively.

In order to predict numerically the acoustic attenuation of expansion chambers with extended inlet/outlet ducts by the boundary element method, the multi-domain approach is necessary because of the presence of a singular boundary [16]. As an effective multi-domain boundary element approach, the substructure boundary element–transfer impedance matrix technique is employed in this study. A detailed description of this technique is provided elsewhere [17].

4. RESULTS AND DISCUSSION

For all configurations, the present study considers $d = 15{\cdot}32$ cm for the chamber diameter, $d_1 = d_2 = 4{\cdot}86$ cm for the inlet/outlet ducts, and two chamber lengths with $l = 28{\cdot}23$ cm and $l = 40{\cdot}84$ cm. These dimensions match those of two concentric expansion chambers in reference [2]. In order to determine analytically the acoustic attenuation of expansion chambers with extended inlet/outlet, the eigenvalues α_n, β_n, γ_n in equations (13)–(15) and (22)–(24) need to be

TABLE 1

The values of α_n, β_n, γ_n *for* $d = 15{\cdot}32$ cm *and* $d_1 = d_2 = 4{\cdot}86$ cm

n	1	2	3	4	5
α_n	3·832	7·016	10·174	13·324	16·470
β_n	4·807	9·322	13·887	18·468	23·057
γ_n	4·807	9·322	13·887	18·468	23·057

obtained first. These eigenvalues are evaluated numerically from equation (4) and are given in Table 1.

Figures 2–4 for $l = 28{\cdot}23$ cm compare the transmission loss for different lengths of extended ducts (Figure 2: $l_1 = 8{\cdot}0$ cm, $l_2 = 0$ cm; Figure 3: $l_1 = 0$ cm, $l_2 = 4{\cdot}0$ cm; Figure 4: $l_1 = 8{\cdot}0$ cm, $l_2 = 4{\cdot}0$ cm). The fundamental behavior will be discussed first in terms of analytical results. The first two resonant peaks in Figure 4 match those in Figures 2 and 3 because the lengths of extended inlet and outlet ducts in Figure 4 are a combination of lengths in Figures 2 and 3. The transmission loss of expansion chambers with extended inlet/outlet ducts exhibit a superposition of domes and resonance peaks in the plane wave region. The number of basic domes (by ignoring the resonances momentarily) increases as the length of the expansion chamber is increased and satisfies equation (28) of reference [2], which is supported by Figures 2 and 5 (Figure 2: $l = 28{\cdot}23$ cm, 4 domes; Figure 5: $l = 40{\cdot}84$ cm, 6 domes). The resonances are due to the extended inlet/outlet ducts. As the lengths of the extended ducts are increased,

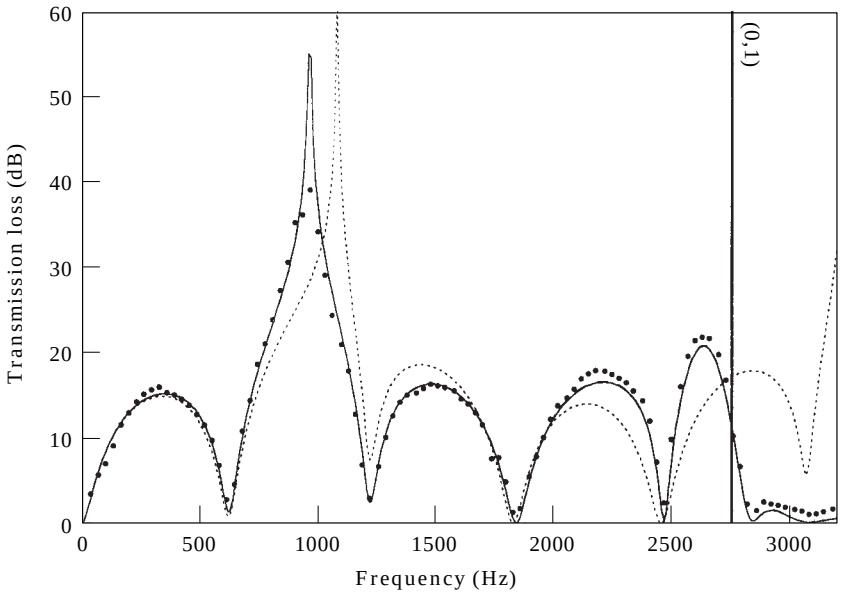

Figure 2. Transmission loss of concentric expansion chamber with extended inlet/outlet; $l = 28{\cdot}23$ cm, $l_1 = 8{\cdot}0$ cm, $l_2 = 0$ cm: ——, 2-D analytical; ●, experimental; – – –, BEM; ·····, 1-D analytical.

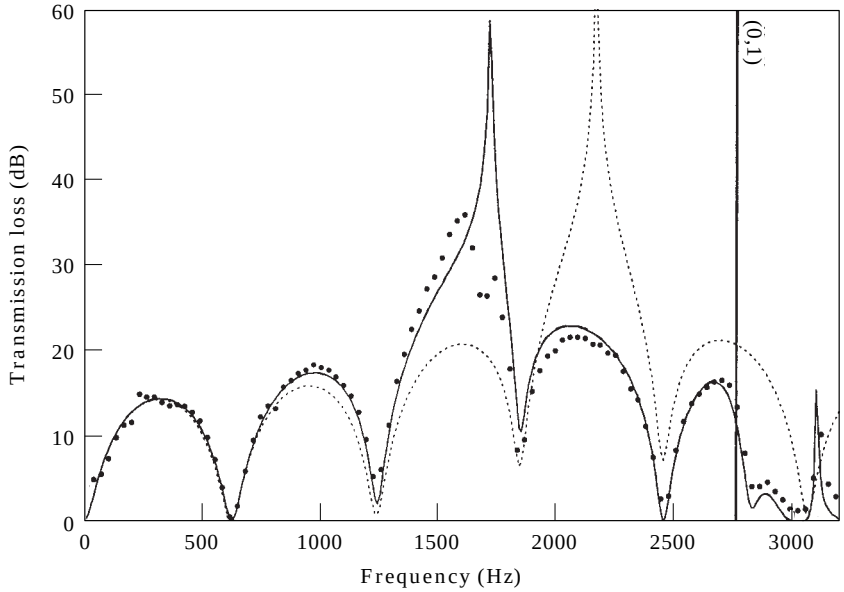

Figure 3. Transmission loss of concentric expansion chamber with extended inlet/outlet; $l = 28{\cdot}23$ cm, $l_1 = 0$ cm, $l_2 = 4{\cdot}0$ cm: ——, 2-D analytical; ●, experimental; – – –, BEM; · · · · · ·, 1-D analytical.

for example, from $l_1 = 8{\cdot}0$ cm of Figure 2 to $l_1 = 12{\cdot}0$ cm of Figure 6, the number of resonance peaks increases and the resonance frequencies are lowered.

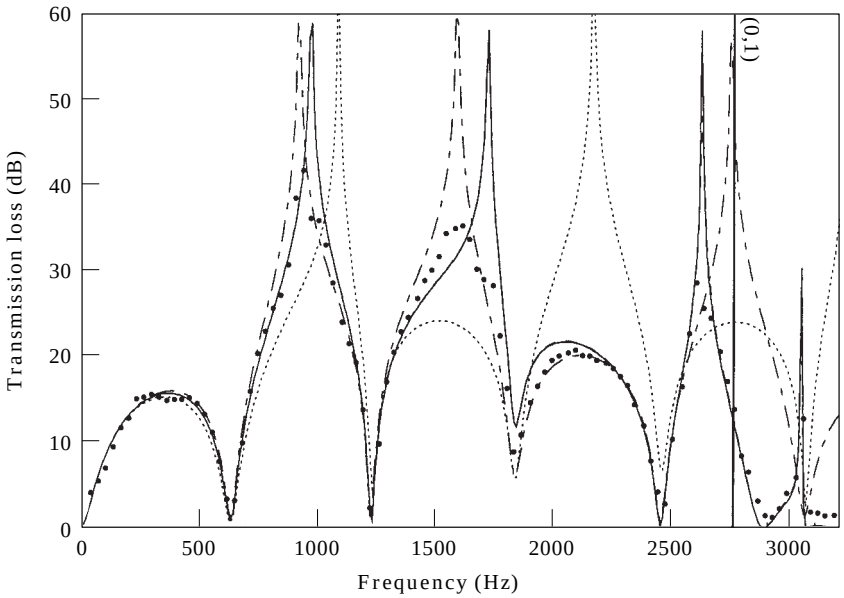

Figure 4. Transmission loss of concentric expansion chamber with extended inlet/outlet; $l = 28{\cdot}23$ cm, $l_1 = 8{\cdot}0$ cm, $l_2 = 4{\cdot}0$ cm: ——, 2-D analytical; ●, experimental; – – –, BEM; · · · · · ·, 1-D analytical; – · – · –, 1-D analytical (with end correction).

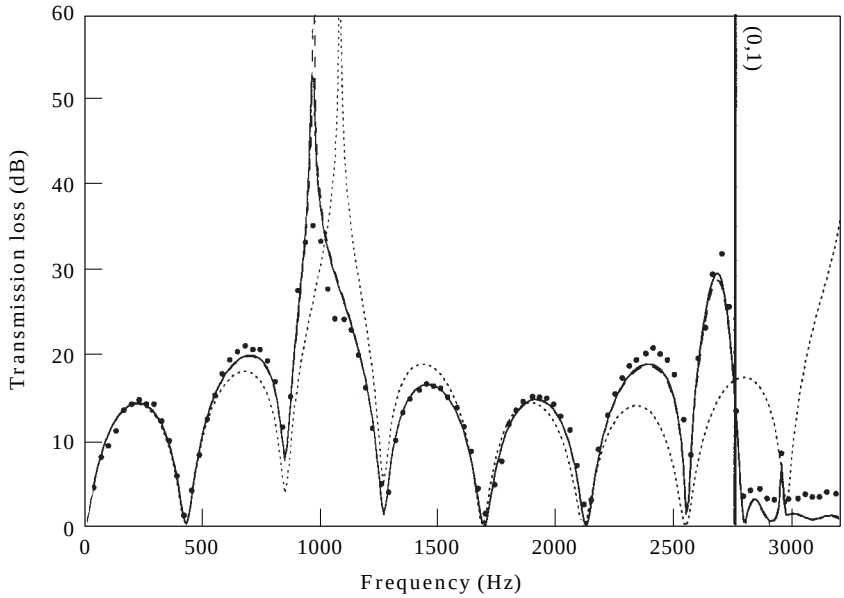

Figure 5. Transmission loss of concentric expansion chamber with extended inlet/outlet; $l = 40{\cdot}84$ cm, $l_1 = 8{\cdot}0$ cm, $l_2 = 0$ cm: ——, 2-D analytical; ●, experimental; – – –, BEM; · · · · · ·, 1-D analytical.

The lengths of extended ducts may be chosen such that the resonances are located at zero-attenuation frequencies of expansion chambers (the troughs, for example, for an expansion chamber with no extensions and $l = 28{\cdot}23$ cm, are

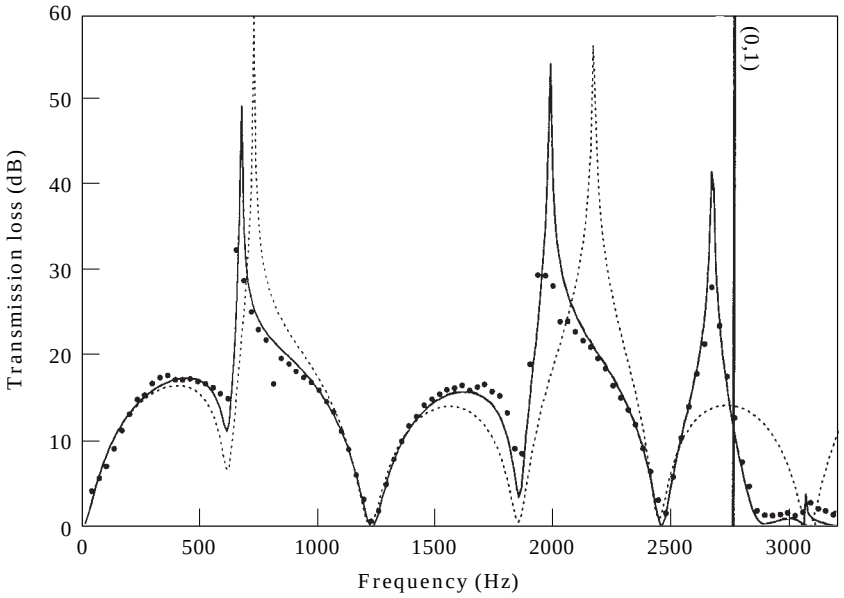

Figure 6. Transmission loss of concentric expansion chamber with extended inlet/outlet; $l = 28{\cdot}23$ cm, $l_1 = 12{\cdot}0$ cm, $l_2 = 0$ cm: ——, 2-D analytical; ●, experimental; – – –, BEM; · · · · · ·, 1-D analytical.

located at 618, 1236, 1854 and 2471 Hz; the speed of sound is 346·1 m/s which is also used in the computational study) leading to a desirable high acoustic attenuation as illustrated in Figure 7 (l_1 = 13·1 cm, l_2 = 6·1 cm). The length l_1 is chosen to match the first trough at 618 Hz and l_2 the second one at 1236 Hz. This behavior demonstrates the benefit of the extended inlet and outlet ducts in the muffler design.

Figures 2–7 compare the transmission loss results from the analytical, computational and experimental approaches. The present analytical approach and the BEM yield nearly identical results throughout the frequency range of interest, and both also agree, in general, with the experimental results. Some deviation from experimental results is observed, for example, near the resonance peak of the shorter extension configuration of Figure 3, and near the resonances of Figure 7. These minor discrepancies are currently being assessed in relation to the neglected viscous effects and the wall thickness of extended ducts in the analytical and computational approaches, and minor geometrical imperfections in the experimental set-up (for example, the slight deviation of the extended ducts from circular cross-section).

Also included in Figures 2–7 are the predictions from equation (26) of simple one-dimensional (1-D) theory. In general, no end correction is used for the ducts in the 1-D approach, with the exception of Figures 4 and 8. The plane wave cut-off frequency of the hollow chamber (see chamber C in Figure 1) is lower than that of an annular chamber (chambers B and D), as illustrated in Table 1. Thus, the cut-off frequency of the hollow chamber determines the region of approximate one-dimensional propagation. When the frequency is higher than

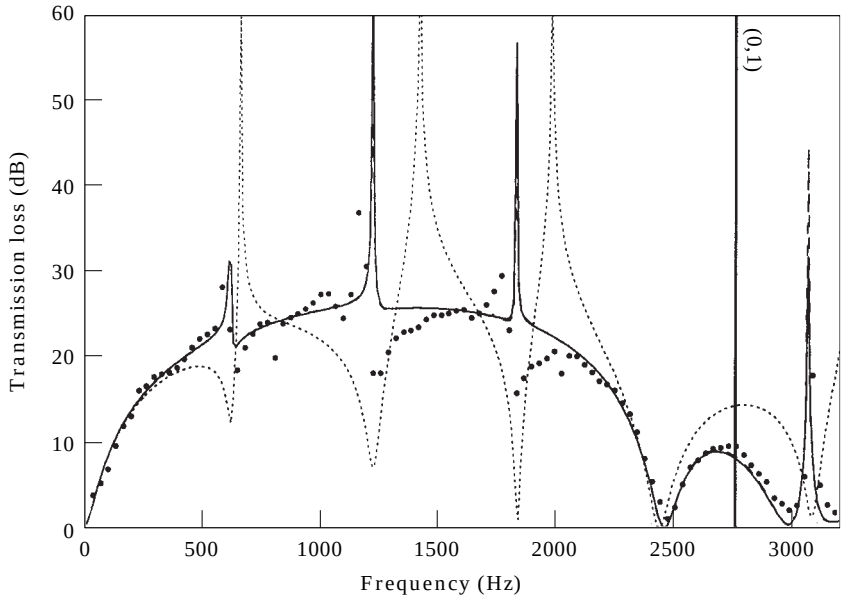

Figure 7. Transmission loss of concentric expansion chamber with extended inlet/outlet; l = 28·23 cm, l_1 = 13·1 cm, l_2 = 6·1 cm: ——, 2-D analytical; ●, experimental; – – –, BEM; · · · · · ·, 1-D analytical.

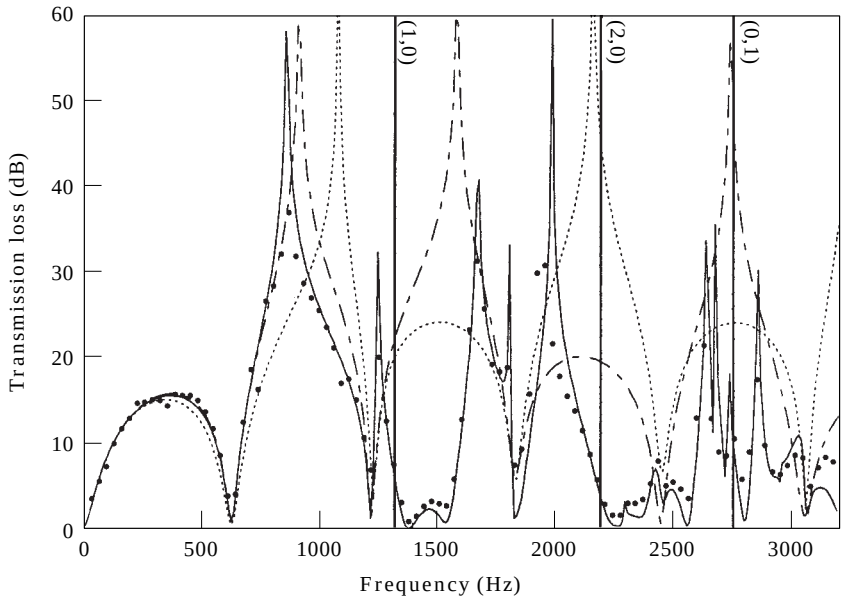

Figure 8. Transmission loss of asymmetric expansion chamber with extended inlet/outlet; $l = 28{\cdot}23$ cm, $l_1 = 8{\cdot}0$ cm, $l_2 = 4{\cdot}0$ cm, 5·1 cm offset inlet, 5·1 cm offset outlet, 180° separation: ●, experimental; ——, BEM; ·····, 1-D analytical; –·–·–, 1-D analytical (with end correction).

the plane wave cut-off frequency of the hollow chamber, the higher order modes are excited, resulting in a dramatic reduction in the acoustic attenuation of expansion chambers with extended ducts, as illustrated in Figures 2–7 beyond the first radial mode (0, 1). Below the plane wave cut-off frequency, the simple 1-D approach may be useful for an approximate estimation of the first resonant peaks for longer duct extensions at relatively low frequencies. The uncorrected 1-D approach misses, however, specifically the resonant peaks of shorter extensions (see Figure 3), and, in general, higher frequency resonances (see Figures 6 and 7). Clearly, for shorter extensions, the end correction such as [1] $\Delta l_{1,2} = 0{\cdot}6a_{1,2} = 1{\cdot}458$ cm becomes rather significant. Applying such correction to both extensions of Figure 4, for example, improves the ability of the 1-D approach to predict resonances below the cut-off frequency.

Similar to the simple expansion chamber without extensions [5], the offset inlet/outlet will excite higher order asymmetric modes and can significantly affect the acoustic attenuation of expansion chambers with extended inlet/outlet. In Figures 8 and 9, the boundary element predictions, as well as the experimental results, are depicted for the expansion chambers with offset extended inlet/outlet of 180° and 90° apart, respectively. For the 180° offset inlet/outlet, the effective acoustic attenuation region is observed until the first diametral (1, 0) mode. For illustrative purposes, 1-D results without and with end correction $\Delta l_{1,2} = 0{\cdot}6a_{1,2}$ are also included in Figure 8. While the end correction helps improve the first order estimate of resonance locations below (1, 0) mode, the 1-D approach including end correction clearly fails above the (1, 0) mode, where the multidimensional approach such as the one presented in this work should be

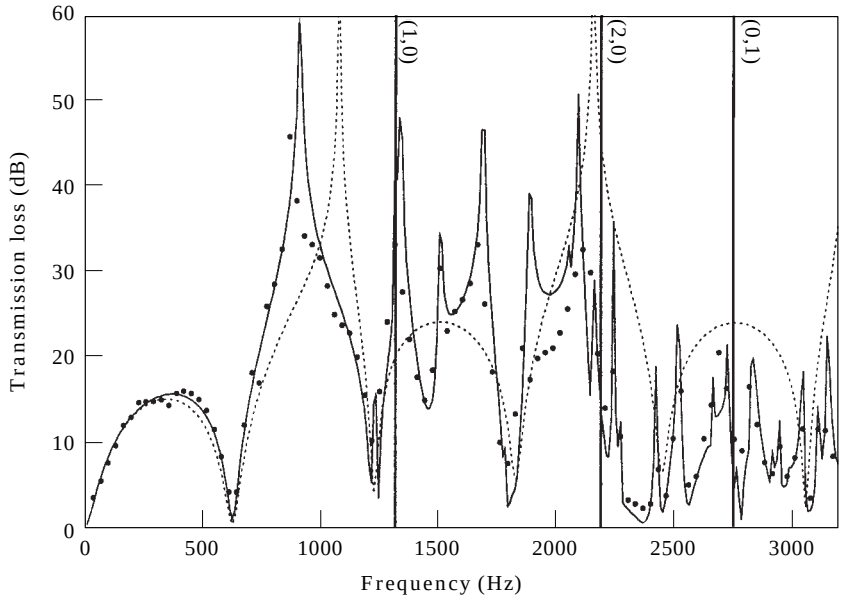

Figure 9. Transmission loss of asymmetric expansion chamber with extended inlet/outlet; $l = 28{\cdot}23$ cm, $l_1 = 8{\cdot}0$ cm, $l_2 = 4{\cdot}0$ cm, 5·1 cm offset inlet, 5·1 cm offset outlet, 90° separation: ●, experimental; ——, BEM; · · · · · · , 1-D analytical.

employed. The detrimental effect of the diametral mode could partially be eliminated by placing the inlet and outlet 90° apart. The results are shown in Figure 9, which exhibit increased transmission loss over the 180° case, particularly in the frequency range between the (1, 0) and (2, 0) modes. The relative behavior of the concentric, 180° offset, and 90° offset extended inlet/outlet configurations may best be illustrated by combining the boundary element results from Figures 4, 8 and 9 in Figure 10.

5. CONCLUDING REMARKS

A two-dimensional analytical approach is presented for the prediction of the acoustic attenuation performance of circular concentric expansion chambers with extended inlet/outlet, and compared with the boundary element predictions and experiments. The effect of the lengths of extended ducts and expansion chambers are investigated analytically, numerically and experimentally for the *concentric* configurations. The expansion chambers with extended inlet/outlet exhibit the combination of the broadband domes and the resonant peaks below the cut-off frequency of the first excited higher order mode of the hollow chamber. The number of domes is the same as the simple expansion chambers and increases as the length of the chamber increases. The number of resonant peaks increases and the resonant frequencies decrease as the length of the extended ducts are increased. By choosing the length of extended ducts to match the resonances with the zero-attenuation frequencies of expansion chambers an

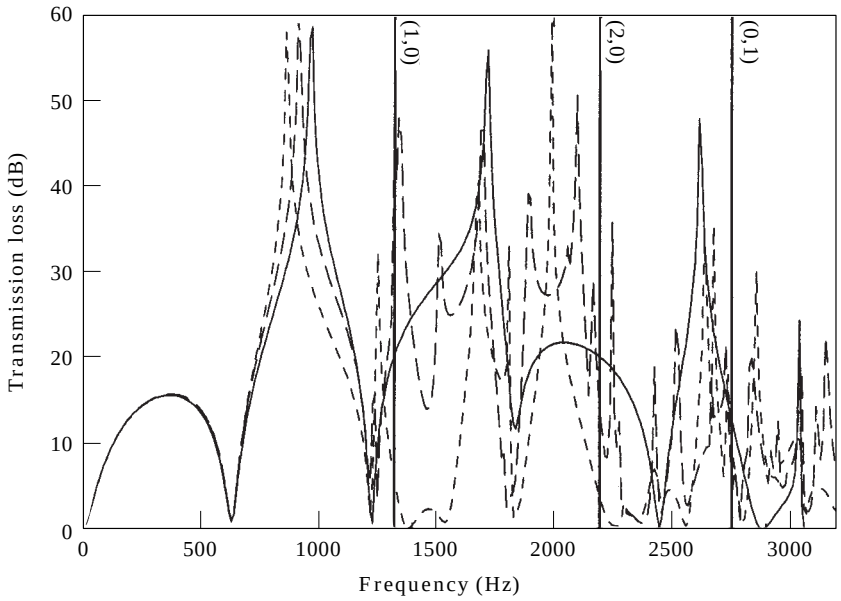

Figure 10. Transmission loss comparison of expansion chamber with extended inlet/outlet; $l = 28{\cdot}23$ cm, $l_1 = 8{\cdot}0$ cm, $l_2 = 4{\cdot}0$ cm, 5·1 cm offset inlet, 5·1 cm offset outlet: ——, concentric configuration; – – –, 180° separation; — —, 90° separation.

excellent acoustic attenuation may be obtained. This behavior demonstrates the advantage of the extended inlet and outlet in the muffler design.

The boundary element predictions and the experimental results for the *asymmetric* configurations show that the effective acoustic attenuation frequency band is observed until the first diametral (1, 0) mode for the 180° offset inlet/outlet, and placing the inlet and outlet 90° apart can improve transmission loss over the 180° case, particularly in the frequency range between the (1, 0) and (2, 0) modes. The accuracy and the bounds of applicability of the 1-D approach with and without end correction are also assessed in comparison with multidimensional techniques at low as well as high frequencies.

REFERENCES

1. M. L. Munjal 1987 *Acoustics of Ducts and Mufflers*. New York: Wiley-Interscience.
2. A. Selamet and P. M. Radavich 1997 *Journal of Sound and Vibration* **201**, 407–426. The effect of length on the acoustic attenuation performance of concentric expansion chambers: an analytical, computational, and experimental investigation.
3. A. I. El-Sharkawy and A. H. Nayfeh 1978 *Journal of the Acoustical Society of America* **63**, 667–674. Effect of the expansion chamber on the propagation of sound in circular pipes.
4. L. J. Erikkson 1980 *Journal of the Acoustical Society of America* **68**, 545–550. Higher order mode effects in the circular ducts and expansion chambers.
5. L. J. Eriksson 1982 *Journal of the Acoustical Society of America* **72**, 1208–1211. Effect of inlet/outlet locations on higher order modes in silencers.

6. A. SELAMET and Z. L. JI 1998 *Journal of Sound and Vibration* **213**, 601–617. Acoustic attenuation performance of circular expansion chambers with offset inlet/outlet: I. Analytical approach.
7. A. SELAMET, Z. L. JI and P. M. RADAVICH 1998 *Journal of Sound and Vibration* **213**, 619–641. Acoustic attenuation performance of circular expansion chambers with offset inlet/outlet: II. Comparison with experimental and computational studies.
8. J. G. IH and B. H. LEE 1985 *Journal of the Acoustical Society of America* **77**, 1377–1388. Analysis of higher-order mode effects in the circular expansion chamber with mean flow.
9. J. KIM and W. SOEDEL 1989 *Journal of Sound and Vibration* **129**, 237–254. General formulation of four pole parameters for three-dimensional cavities utilizing modal expansion, with special attention to the annular cylinder.
10. A. D. SAHASRABUDHE, M. L. MUNJAL and S. A. RAMU 1992 *Noise Control Engineering Journal* **38**, 27–38. Design of expansion chamber mufflers incorporating 3-D effects.
11. A. SELAMET and Z. L. JI 1998 *Journal of the Acoustical Society of America* **104**, 2867–2877. Acoustic attenuation performance of circular flow-reversing chambers.
12. J. G. IH and B. H. LEE 1987 *Journal of Sound and Vibration* **112**, 261–273 Theoretical investigation of flow-reversing chamber.
13. A. SELAMET, P. M. RADAVICH, N. S. DICKEY and J. M. NOVAK 1997 *Journal of the Acoustical Society of America* **101**, 41–51. Circular concentric Helmholtz resonators.
14. M. ÅBOM 1990 *Journal of Sound and Vibration* **137**, 403–418. Derivation of four-pole parameters including higher order mode effects for expansion chamber mufflers with extended inlet and outlet.
15. A. D. SAHASRABUDHE, S. A. RAMU and M. L. MUNJAL 1991 *Journal of Sound and Vibration* **147**, 371–394. Matrix condensation and transfer matrix techniques in the 3-D analysis of expansion chamber mufflers.
16. C. Y. R. CHENG and A. F. SEYBERT 1991 *Journal of Sound and Vibration* **151**, 119–129. A multidomain boundary element solution for silencer and muffler performance prediction.
17. Z. L. JI, Q. MA and Z. H. ZHANG 1994 *Journal of Sound and Vibration* **173**, 57–71. Application of the boundary element method to predicting acoustic performance of expansion chamber mufflers with mean flow.
18. A. CUMMINGS 1975 *Journal of Sound and Vibration* **41**, 375–379. Sound transmission in a folded annular duct.
19. M. K. AU-YANG 1979 *Journal of Sound and Vibration* **62**, 577–591. Pump induced acoustic pressure distribution in an annular cylinder.
20. M. ABRAMOWITZ and I. A. STEGUN 1970 *Handbook of Mathematical Functions*. New York: Dover.

APPENDIX A: INTEGRALS IN EQUATIONS (13)–(15) AND (22)–(24)

The integral relations [20] for Bessel function $B_n(x)$ of any kind and order n give

$$\int rB_0(\lambda r)B_0(\mu r)\,\mathrm{d}r = \begin{cases} \dfrac{r}{\lambda^2-\mu^2}\{\lambda B_1(\lambda r)B_0(\mu r) - \mu B_0(\lambda r)B_1(\mu r)\}, & (\lambda \neq \mu), \\ \dfrac{r^2}{2}\{B_0^2(\lambda r) + B_1^2(\lambda r)\}, & (\lambda = \mu). \end{cases} \tag{A1}$$

The integrals in equations (13)–(15) and (22)–(24) may then be evaluated as

$$\langle \Psi_{A,s}\Psi_{A,s}\rangle_A = a_1^2 J_0^2(\alpha_s), \tag{A2}$$

$$\langle \Psi_{B,s}\Psi_{B,s}\rangle_B = a^2 \Psi_{B,s}^2(a) - a_1^2 \Psi_{B,s}^2(a_1), \tag{A3}$$

$$\langle \Psi_{C,s}\Psi_{C,s}\rangle_C = a^2 J_0^2(\alpha_s), \tag{A4}$$

$$\langle \Psi_{D,s}\Psi_{D,s}\rangle_D = a^2 \Psi_{D,s}^2(a) - a_2^2 \Psi_{D,s}^2(a_2), \tag{A5}$$

$$\langle \Psi_{E,s}\Psi_{E,s}\rangle_E = a_2^2 J_0^2(\alpha_s), \tag{A6}$$

$$\langle \Psi_{C,n}\Psi_{A,s}\rangle_A = \begin{cases} \dfrac{2\alpha_n a_1/a J_0(\alpha_s) J_1(\alpha_n a_1/a)}{(\alpha_n/a)^2 - (\alpha_s/a_1)^2} & (\alpha_n/a \neq \alpha_s/a_1) \\ a_1^2 J_0^2(\alpha_s) & (\alpha_n/a = \alpha_s/a_1) \end{cases}, \tag{A7}$$

$$\langle \Psi_{C,n}\Psi_{B,s}\rangle_B = \begin{cases} \dfrac{2\alpha_n a_1/a J_1(\alpha_n a_1/a) \Psi_{B,s}(a_1)}{(\beta_s/a)^2 - (\alpha_n/a)^2} & (\alpha_n \neq \beta_s) \\ a^2 \Psi_{C,n}(a)\Psi_{B,s}(a) - a_1^2 \Psi_{C,n}(a_1)\Psi_{B,s}(a_1) & (\alpha_n = \beta_s) \end{cases}, \tag{A8}$$

$$\langle \Psi_{C,n}\Psi_{D,s}\rangle_D = \begin{cases} \dfrac{2\alpha_n a_2/a J_1(\alpha_n a_2/a) \Psi_{D,s}(a_2)}{(\gamma_s/a)^2 - (\alpha_n/a)^2} & (\alpha_n \neq \gamma_s) \\ a^2 \Psi_{C,n}(a)\Psi_{D,s}(a) - a_2^2 \Psi_{C,n}(a_2)\Psi_{D,s}(a_2) & (\alpha_n = \gamma_s) \end{cases}, \tag{A9}$$

$$\langle \Psi_{C,n}\Psi_{E,s}\rangle_E = \begin{cases} \dfrac{2\alpha_n a_2/a J_0(\alpha_s) J_1(\alpha_n a_2/a)}{(\alpha_n/a)^2 - (\alpha_s/a_2)^2} & (\alpha_n/a \neq \alpha_s/a_2) \\ a_2^2 J_0^2(\alpha_s) & (\alpha_n/a = \alpha_s/a_2) \end{cases}. \tag{A10}$$

APPENDIX B: NOMENCLATURE

A_n, B_n, C_n, D_n, E_n	modal amplitudes in regions A, B, C, D, E (see Figure 1)
a, a_1, a_2	radii of expansion chamber, inlet, and outlet ducts
J_0, J_1	Bessel functions of the first kind of order 0 and 1
$k_{A,n}$	$=[k^2-(\alpha_n/a_1)^2]^{1/2}$, axial wavenumber in region A
$k_{B,n}$	$=[k^2-(\beta_n/a)^2]^{1/2}$, axial wavenumber in region B
$k_{C,n}$	$=[k^2-(\alpha_n/a)^2]^{1/2}$, axial wavenumber in region C
$k_{D,n}$	$=[k^2-(\gamma_n/a)^2]^{1/2}$, axial wavenumber in region D
$k_{E,n}$	$=[k^2-(\alpha_n/a_2)^2]^{1/2}$, axial wavenumber in region E
l, l_1, l_2	length of expansion chamber, extended inlet, and outlet ducts
n	mode number

P	acoustic pressure
q	number of terms after truncation
s	orthogonal expansion terms
S_A, S_B, S_C, S_D, S_E	cross-sectional areas of regions A, B, C, D, E
U	particle velocity
Y_0, Y_1	Bessel functions of the second kind of order 0 and 1
α_n	zeros of $J_1(\alpha_n)=0$ (hollow duct C)
β_n	zeros of $J_1(\beta_n a_1/a)-[J_1(\beta_n)/Y_1(\beta_n)]Y_1(\beta_n a_1/a)=0$ (annular duct B)
γ_n	zeros of $J_1(\gamma_n a_2/a)-[J_1(\gamma_n)/Y_1(\gamma_n)]Y_1(\gamma_n a_2/a)=0$ (annular duct D)
$\Psi_{A,n}(r)$	$=J_0(\alpha_n r/a_1)$, for region A
$\Psi_{B,n}(r)$	$=J_0(\beta_n r/a)-[J_1(\beta_n)/Y_1(\beta_n)]Y_0(\beta_n r/a)$, for region B
$\Psi_{C,n}(r)$	$=J_0(\alpha_n r/a)$, for region C
$\Psi_{D,n}(r)$	$=J_0(\gamma_n r/a)-[J_1(\gamma_n)/Y_1(\gamma_n)]Y_0(\gamma_n r/a)$, for region D
$\Psi_{E,n}(r)$	$=J_0(\alpha_n r/a_2)$, for region E
Δl_1, Δl_2	end corrections for the extended inlet/outlet ducts